Wetting dynamics in two-liquid systems: Effect of the surrounding phase viscosity

P. Bazazi,[1,2] A. Sanati-Nezhad,[2,3] and S. H. Hejazi[1,*]

[1]*Porous Media Laboratory, Chemical and Petroleum Engineering, University of Calgary, Calgary, Alberta, Canada T2N 1N4*

[2]*BioMEMS and Bioinspired Microfluidic Laboratory, Department of Mechanical and Manufacturing Engineering, University of Calgary, Calgary, Alberta, Canada T2N 1N4*

[3]*Centre for Bioengineering Research and Education, University of Calgary, Calgary, Alberta, Canada T2N 1N4*

(Received 31 December 2017; published 13 June 2018)

This paper reports the experimental results of a water droplet spreading on a glass substrate submerged in an oil phase. The radius of the wetted area grows exponentially over time forming two distinct regimes. The early time dynamics of wetting is characterized with the time exponent of 1, referred to as the viscous regime, which is ultimately transitioned to the Tanner's regime with the time exponent of 0.1. It is revealed that an increase in the ambient phase viscosity over three decades considerably slows down the rate of three-phase contact line movement. A scaling law is developed where the three-phase contact line velocity is a function of both spreading radius and mean viscosity, close to the geometric mean of the droplet and ambient fluids' viscosities. Using the proposed scaling and mean viscosity, all plots of spreading radius for different viscosity ratios collapse to a master curve. Furthermore, several cases with multiple rupture and spreading points, i.e., wetting in a nonideal system, are considered. The growth of an equivalent wetting radius in a multiple point spreading system is predicted by the developed scaling law.

DOI: 10.1103/PhysRevE.97.063104

I. INTRODUCTION

A liquid drop spreading on solid surfaces is a common phenomenon in natural and engineering processes of biosurfaces [1], oil recovery [2–5], emulsification [6,7], oil-water filtration, detergency [8,9], and printing and coating [10,11]. Wetting is the interaction among three phases: two fluids that are competing to cover a solid substrate. When a droplet touches a solid surface, a highly curved meniscus forms at the contact point driving the spherical liquid droplet on to wet the surface. Spreading of liquid droplets initiates from the unbalanced interfacial forces and ultimately approaches an equilibrium where the driving forces are balanced with the viscous dissipation [12–14]. The final shape of the drop (a spherical cap geometry) is characterized using the equilibrium contact angle as expressed in Young's equation.

The wetting dynamics, i.e., the early and late times of liquid drop spreading, have been the focus of many studies. Several predictive models based on molecular kinetic theory or hydrodynamic theory investigate the late time behavior of the contact line motion close to the equilibrium [15–17]. This process is well understood due to the ease of experiments and well established theoretical works; the drop contact line moves as a function of $r \sim t^{0.1}$ referring to Tanner's law [17]. r and t are the equivalent radius of the wetted area and time, respectively. The late time dynamics of drop spreading is reported in many studies on the low-viscosity (inviscid) ambient phase (gas) [9,18–21]. Other studies explore the spreading in a second viscous fluid phase [22–24]. In a pioneering set of experiments, Foister [25] studied the drop spreading on a solid surface in the presence of a liquid medium. The three-phase boundary motion is a function of the droplet itself, ambient phase viscosities, and interfacial tension of fluids. In other work, Foister [26] studied the influence of physical properties of liquid-liquid-solid systems (viscosity ratios, interfacial tension, and dynamic contact angle) on the late time movement of the contact line. The validity of Tanner's law for the cases with a non-negligible surrounding phase viscosity was demonstrated. It was shown that for a constant contact angle, the contact line velocity decreases as the ratio of droplet viscosity to that of the surrounding liquid increases [26].

The drop shape after the contact is highly curved close to the contact point, similar to the coalescence of two identical droplets [14,27,28]. Upon two drops coalescing, a bridge forms where the capillary forces are the main driving force for the bridge radius expansion. The capillary forces eventually balance due to the viscous or inertial forces. The strongly curved meniscus at the contact point generates a rapid flow inside the drop initiating its coalescence and spreading. From a theoretical point of view, the coalescence of drops may start from a viscosity-dominated regime with a power law behavior in the form of $r \sim t \ln t$ for a coalescence in an inviscid ambient phase [29]. The growth rate of the contact radius reduces by a factor of 4 where the coalescence occurs in a viscous fluid instead of an inviscid one [30]. The experiments confirm that the coalescence starts from a viscosity-dominated regime where the contact radius linearly increases with time as $r \sim t$ [31,32]. Following the initial viscous regime, the inertial forces are dominant in the second stage of the coalescence where $r \sim \sqrt{t}$ [31,33,34]. The effect of ambient phase viscosity on the air bubble and liquid drop coalescence has recently been studied [35]. The significance of the outer fluid properties in the coalescence dynamics is characterized by a dimensionless Ohnesorge number ($\mu_{out}/\sqrt{\rho\gamma R}$), where μ_{out} is the viscosity of the outer fluid, ρ is the density of the denser fluid, γ is surface

*Corresponding author: shhejazi@ucalgary.ca

tension, and R is the initial drop radius [35]. For $\mu_{out} \gg \mu_{in}$ (μ_{out} is outer fluid viscosity and μ_{in} is drop viscosity), the coalescence dynamics of gas bubbles is always dominated by the outer fluid while only late time dynamics for water drops is dominated by the outer fluid [35].

The spreading-coalescence approach is used to analyze the motion of drop contact line on flat surfaces in a low-viscosity ambient phase, mostly air at atmospheric pressure. The general conclusion is that the droplet spreading in total wetting condition has the same dynamics as the coalescence of identical droplets. Eddi *et al.* [27] examined the role of solid surface wettability, drop size, and drop viscosity on the spreading dynamics in the air. Their experiments found the existence of two distinctive regimes: fast dynamics at the early time and a slow growth of wetted area later on. The early time dynamics is independent from surface hydrophobicity and droplet size. Increasing the drop viscosity slowed down the fast dynamics of spreading. In comparison with earlier studies that characterized the initial time spreading of a low-viscosity drop (water) in the air as an inertial dominant dynamics with $r \sim \sqrt{t}$ [14,36], the spreading radii enlarged in the course of time as $r \sim t^{\alpha}$ with $0.5 < \alpha < 1$ for high-viscosity droplets. Mitra and Mitra [28] investigated the initial stages of liquid drop spreading with viscosities of 16 and 200 mPa s on a flat solid surface surrounded by water. The use of a viscous fluid (i.e., water) instead of gas (i.e., air) as the ambient phase significantly slowed down the spreading process. Hence, the early time events were precisely captured. The spreading started from a viscosity-dominated regime with $r \sim t$ for oil droplets. The spreading of water and oil drops in the air was also initiated from a viscosity-dominant regime.

Most studies focus on spreading dynamics where the drop phase is generally more viscous than the ambient phase. In applications of oil recovery [37], chemical filtration, and CO_2 sequestration [38], spreading occurs in a surrounding liquid with a higher viscosity than that of the drop. It is essential to understand the dependency of wetting dynamics on the relative values of viscosities and densities of the inner (droplet) and outer (ambient) fluids. The spreading dynamics is impacted when the wetting starts from multiple rupture points. To gain insight into how the viscosity of the ambient phase affects the wetting dynamics, visualization experiments for imaging the process of a liquid droplet spreading on a flat solid substrate submerged in another liquid phase with a viscosity equal to or higher than that of the droplet are performed. De-ionized water droplets with the viscosity of 1 mPa s wet a partially hydrophilic glass substrate submerged in oil phases with the viscosities ranging from 0.86 mPa s (slightly smaller than that of water) to 1000 mPa s (three orders of magnitude larger than water). Scaling analysis in terms of the viscosity ratio, radius of wetted area, and capillary number is performed to disclose the relationship between the moving contact line velocity and the viscosities of the inner and outer fluids. A general correlation is sought to predict the expansion of the wetted area. The spreading dynamics in nonideal systems where the wetting starts from multiple rupture points with some residual oil trapped underneath the water droplet is also analyzed.

This paper is organized as follows. In Sec. II, the experimental procedure is introduced and the relevant properties of the fluids and the solid are presented. The experimental data are reported and analyzed in Sec. III. The discussions and conclusions are given in Sec. IV.

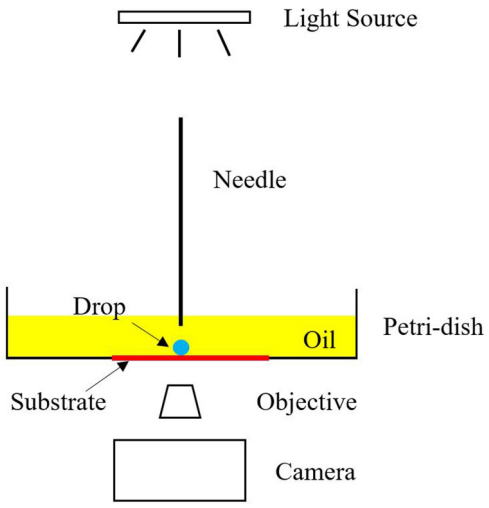

FIG. 1. Schematic of the experimental setup. A Petri dish filled with oil is placed on an inverted microscope coupled with a camera. A drop of water with a volume of 2 μl is injected in the middle of the Petri dish, 7 mm above the glass substrate. The drop moves downward by gravity and spreads over the solid surface.

II. EXPERIMENTS

The spreading rate of water drops on the hydrophilic glass surface submerged in an oil phase is measured. The measurement is based on the analysis of images taken from the bottom of the glass using bottom view imaging. Images with adequate spatial and temporal resolutions capture the initial steps of spreading and the motion of the three-phase contact line. Figure 1 shows the developed setup for the experiments. A Petri dish is filled with oil and placed on an inverted microscope (Nikon A1R) connected to cameras (DS-RI2 and Zyla 4.2 PLUS sCMOS). A droplet of de-ionized water (density of 998.5 kg/m^3 and viscosity of 1.01 mPa s) with a volume of 2 μl is placed within the bulk phase where the oil is about 7 mm above the glass substrate. The droplet sinks until it touches the glass surface. The average descending velocities of droplets in the experiments are below 1 mm s^{-1}. They are smaller than the velocity to impact the spreading dynamics [14]. The droplet spreading dynamics' independence of the submersion time is verified by placing the droplet at various depths of the bulk phase.

Four different oils with viscosities of 0.86, 12, 178, and 1000 mPa s represent the bulk phase including decane (anhydrous grade, Sigma), two types of mineral oils (Sigma and Penreco), and a laser oil (Cargille). Oil-water interfacial tensions and contact angles are measured using the pendant drop and sessile drop methods, respectively. The oils are selected in such a way that the variations in theirs densities (730–900 kg/m^3) and also their interfacial tensions with water (37–44 mN/m) are small. Thus, the oil viscosity is the dominant parameter affecting the spreading dynamics. The glass substrates (Globe Scientific Inc) are used without any treatment. Each glass slide is used for one experiment. Table I summarizes the physical

TABLE I. Physical properties of oil samples.

Oil	Density (kg/m^3)	Viscosity (mPa s)	IFT (mN/m)	Contact angle
Decane	730	0.86	40 ± 1	65 ± 3
Mineral oil	837	12	37 ± 1	67 ± 3
Mineral oil	890	178	42 ± 2	77 ± 2
Laser oil	900	1000	44 ± 2	72 ± 3

properties of the oil samples for density, viscosity, contact angle, and interfacial tension (IFT) values.

The bottom view images are more accurate than the side view ones [27]; therefore the wetting dynamics are recorded from the bottom of the glass in all our experiments. Images are captured with the spatial resolution of 3.68 μm/pixel for every 5 ms. To minimize the effect of vibration, the setup is placed on a vibration isolation table. Once the falling droplet touches the solid surface, a circular area wetted by water is formed. The recorded wetted areas are processed using the IMAGE FIJI package (IMAGEJ). Each experiment is repeated at least five times to ensure the reproducibility of experimental data. The main uncertainty in data analysis is related to the very first few images captured where the wetted area covers only a couple of pixels of the image.

III. RESULTS AND DISCUSSION

A. Droplet spreading

The impact of the surrounding fluid viscosity on the spreading dynamics is investigated to capture the motion of three-phase contact lines. A water droplet with the initial radius of $R = 780 \pm 20$ μm spreads on the hydrophilic glass substrate immersed in an oil phase. Wetting occurs from a single rupture point and expands in a geometry close to a circle (see Fig. S1 in the Supplemental Material [39] for the bottom view images of the droplet spreading). The radius of the growing circles, r, is measured and used as the basis for the analysis of wetting dynamics. Figure 2(a) illustrates the evolution of r as a function of time for different viscosity ratios. The spreading starts with a sharp slope approaching a plateau in a few seconds. The spreading slows down over time and eventually all drops reach approximately the same radius representing the equilibrium three-phase contact angle.

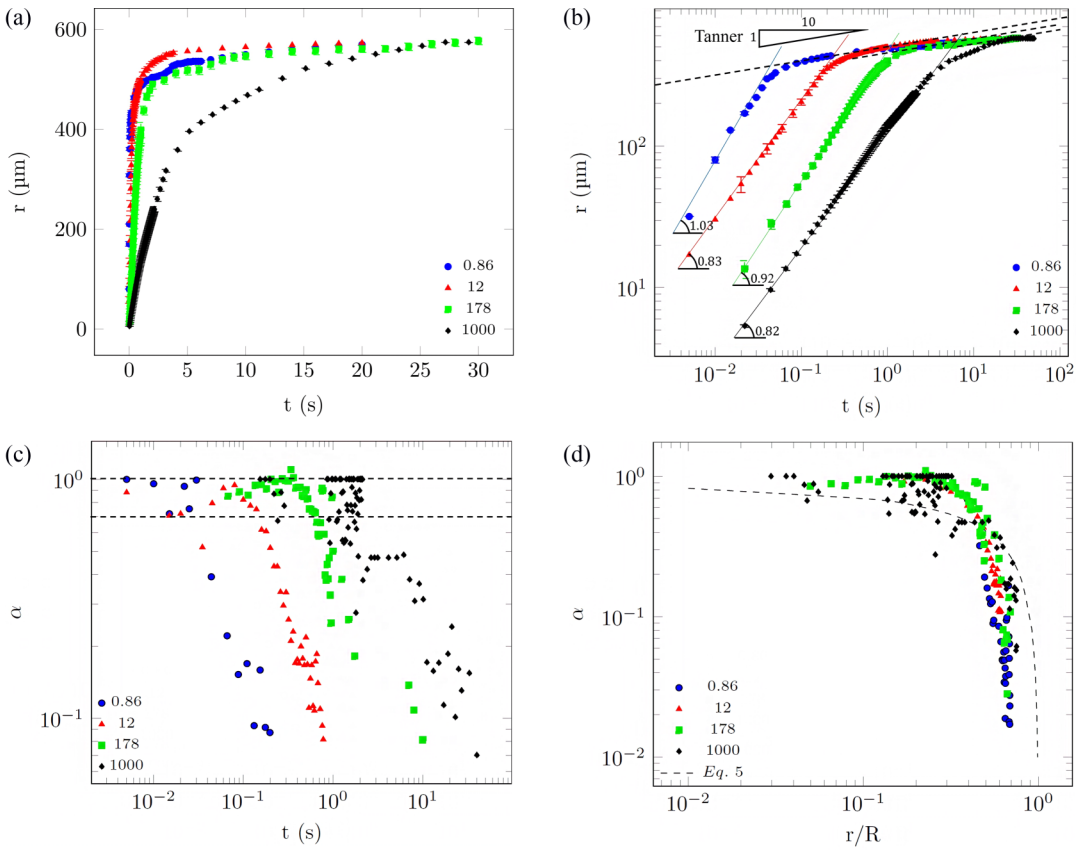

FIG. 2. (a) Spreading radius (r) as a function of time for the spreading of aqueous drops under the oil phase with different viscosity ratios, 0.86, 12, 178, and 1000, in blue, red, green, and black, respectively. Increasing the viscosity of the outer fluid decreases the rate of spreading. All curves have a sharp slope at the initial time reaching a plateau. (b) The evolution of r as a function of t in log-log scale. The initial dynamics is identical within the experimental error. Embedded triangles show the slopes. Lines passing through the data points in the first regime are only a visual guide. The black dashed line passing through the late time data has the slope of 0.1. (c) Evolution of measured apparent exponent α as a function of time for the same data as in (b). (d) Evolution of α as a function of r/R for the same data as in (b). The black dashed line is the prediction from Eq. (1).

By contrast, in the early time, the contact line movements are fast. Figure 2(a) reveals that the rate of spreading decreases by increasing the viscosity of the ambient phase. The motion of the three-phase contact line depends on the droplet curvature next to the contact point. This is characterized by the thickness of the thin film of oil lying between the water and solid surface [25]. The film thickness depends on the initial droplet size and viscosity ratios between the two liquids [25]. The volume of the water droplet is preserved in each experiment. The gap between the droplet and solid surface and the contact line movement are dependent on the viscosity ratio.

The rapid dynamics of spreading at the early stage is best illustrated in log-log scale Fig. 2(b). For $\mu_{out}/\mu_{in} \ll 1$, when the outer fluid is water [28] or gas [13,26,40], the spreading dynamics follows a power-law behavior in the form of $r \sim t^{\alpha}$. To investigate whether these experiments with $\mu_{out}/\mu_{in} \geqslant 1$ display the power-law spreading regimes, the apparent exponent ($\alpha = d\ln r/d\ln t$) is plotted as a function of time (t) and the spreading radius is scaled with the initial droplet radius (r/R). Figure 2(c) depicts the evolution of α as a function of time for four different viscosity ratios. At the initial time, there is a fast dynamic with an exponent $0.8 < \alpha < 1$ where the duration is directly related to the viscosity ratio. α decreases in all scenarios and becomes stabilized in a value close to 0.1, consistent with the Tanner's regime. By plotting α as a function of r/R in Fig. 2(d), all the curves collapse to a single one. The effective exponent of viscous drop coalescence suggested by Eddi *et al.* [27] is calculated as in Eq. (1):

$$\alpha = \frac{\ln\left(\frac{r}{R}\right)}{\ln\left(\frac{r}{R}\right) - 1}. \tag{1}$$

The predicted exponents using Eq. (1) are embedded in Fig. 2(d) by the black dashed line. The experimental and predicted values of α follow the same trends. The plot reveals that the experimental exponents are closer to 1 than those from Eq. (1). A rapid decline to 0.1 occurs at $r/R \geqslant 0.4$. It should be noted that Eq. (1) provides a stronger prediction for the viscous droplet spreading in an outer fluid with a negligible viscosity [27]. In all viscosity ratios, α decreases with time and dimensionless radius. In Fig. 2(c), deviations of α from the values close to 0.8–1 (dashed horizontal lines embedded in the plot) represent the transition from the viscous regime. The transition time increases as the outer fluid viscosity increases. All the curves in Fig. 2(d) collapse in one curve, meaning that the transition radius is less sensitive to the viscosity ratio. For this set of experiments, the spreading changes from one regime to another at the dimensionless radius of about $r/R = 0.4$.

For all viscosity ratios, three distinct regimes are characterized based on the values of spreading exponent in Figs. 2(a)–2(d). The droplet spreading starts with a fast dynamic with the spreading exponent of $0.8 < \alpha < 1$. This fast dynamic is similar to the drop coalescence, referred to as the viscosity-dominated regime where the spreading radius grows as $r \sim t$. The process then follows a transition regime where $0.1 < \alpha < 0.8$ with an average value of $\alpha \approx 0.5$. The duration of this transition zone is an increasing function of ambient phase viscosity which takes about 0.03 and 8 s for oils with the viscosities of 0.86 and 1000 mPa s, respectively. The spreading exponent ends up with values close to 0.1, as predicted by Tanner's regime. The transition time from one regime to another can be distinguished using the changes in the spreading exponents.

B. Scaling system

Dimensional analysis. Considering Fig. 2(a), the velocity of the contact line (rate of the spreading) is dependent on the viscosity ratio between the two fluids. The rate of spreading is a decreasing function of the spreading radius. The other governing factor is the interfacial tension as the main driving force for the radius expansion. Thus, the three-phase contact line velocity ($U = dr/dt$) can be written as Eq. (2):

$$U = U(\mu_{in}, \mu_{out}, \gamma, R, r). \tag{2}$$

Dimensional analysis based on the Buckingham π theorem results in three dimensionless groups governing the expansion of the wetting line as in Eq. (3):

$$\pi_1 = \frac{\mu_{out} U}{\gamma}, \quad \pi_2 = \frac{\mu_{out}}{\mu_{in}}, \quad \pi_3 = \frac{r}{R}, \tag{3}$$

where π_1 is the capillary number (Ca), the ratio of viscous forces to capillary forces. Other combinations of dimensionless groups can be found using π_1,π_2, and π_3. Considering the viscosity ratio and spreading radius as the main independent factors, we can write

$$\pi_1 = C\pi_2^A \pi_3^B, \tag{4}$$

where A, B, and C are determined by the experimental data when $r/R < 0.4$. Considering the definition of capillary number and slight rearrangements, a correlation for the velocity of the spreading radius is defined in Eq. (5):

$$U = C\frac{\gamma\left(\frac{r}{R}\right)^{-0.43(\mu_{out}/\mu_{in})^{-0.1}}}{\mu_{out}^{\beta}\,\mu_{in}^{1-\beta}}, \tag{5}$$

where C is a constant value (see Fig. S2 in the Supplemental Material [39] for more details). One main finding in the dimensional analysis is the existence of an average viscosity ($\mu_m = \mu_{out}^{\beta}\,\mu_{in}^{1-\beta}$) to scale the spreading phenomenon. The viscosity exponent (β) is 0.53 ± 0.03. Please note the low-viscosity case of 0.86 has a fast spreading dynamics at the early stage. Hence, a limited number of data points are collected for this case. The low frame rate may adversely impact the accuracy of the developed correlations. Thus, we exclude the case of 0.86 from the analysis and evaluate β. It is verified that the viscosity exponent is $\beta = 0.55 \pm 0.01$. The exponent value is very close and in the range of the one predicted using all sets of experiments ($\beta = 0.53 \pm 0.03$) signaling the minimal effect of low-viscosity data in the developed correlations. Although the analysis verifies the validity of the developed correlations for a wide range of viscosity rations, one might opt to exclude the low-viscosity cases. This average viscosity is very close to the geometric mean of inner and outer viscosities $(\mu_{out}\mu_{in})^{0.5}$ where the observed deviation could be the result of experimental errors. The mean viscosity (μ_m) is used for further scaling analysis of the present problem. The dimensionless radius r/R is evaluated by the integration of

Eq. (5):

$$\frac{r}{R} = \left\{ C\left[1 + 0.43\left(\frac{\mu_{\text{out}}}{\mu_{\text{in}}}\right)^{-0.1}\right]\frac{t}{(\mu_m R/\gamma)} \right\}^{\left[1+0.43\left(\mu_{\text{out}}/\mu_{\text{in}}\right)^{-0.1}\right]^{-1}}. \tag{6}$$

Scaling of experimental data. Another important finding of the dimensional analysis is the possibility to develop general scaling parameters that may result in the collapse of all spreading radii into a master curve. A scaling process based on the analogy of the drop coalescence scaling [30,31] is adopted. Considering the viscosity-dominated regime, Eqs. (7) and (8) are written using μ_m in Ca and equating the capillary number to unity.

$$U = \frac{dr}{dt} \sim \frac{\gamma}{\mu_m}, \tag{7}$$

or

$$\frac{r}{R} = C_1 \frac{t}{\mu_m R/\gamma}. \tag{8}$$

Where C_1 is a constant value. The experimental data presented in Fig. 2(b) are scaled using R and $\tau_c = \mu_m R/\gamma$ as the characteristic length and time, respectively. The plot of scaled experimental data (dimensionless radius r/R as a function of dimensionless time t/τ_c) results in a master curve where all data points for different viscosity ratios collapse in that curve as presented in Fig. 3(a). The parameters that change the rate of spreading in different experiments are the mean viscosity and interfacial tension. In this set of experiments, the main variable is the outer fluid viscosity. The drop phase is water in all the experiments and interfacial tension does not have a significant variation between different oil samples and water. Increasing the outer fluid viscosity increases the viscous stress in the surrounding liquid which is the main resistance to the Laplace pressure (driving force for spreading). As a result, increasing the viscosity of the surrounding oil slows down the velocity of water drop spreading. Hence, the data from different experiments collapse into a single master curve that considers the effect of the outer fluid viscosity in the characteristic time scale ($\tau_c = \mu_m R/\gamma$). We calculate r/R based on Eq. (6) and plot the data as a function of t/τ_c for $r/R < 0.4$. The resultant r/R from Eq. (6), shown in Fig. 3(a) with the black dashed line, demonstrates a fair agreement with the experimental data.

The developed scaling procedure is further used to analyze the available experimental data for three cases of glycerin-water droplet spreading in air [27] and two cases of laser oil and dibutyl phthalate droplets spreading in water [28]. For each case, the spreading radius at the viscous regime is scaled by the original droplet radius. We use the inner and outer fluids' viscosities related to each experiment to determine the mean viscosity ($\mu_m = \mu_{\text{out}}^{0.53}\,\mu_{\text{in}}^{0.47}$) and evaluate the characteristic time as $\tau_c = \mu_m R/\gamma$. According to Eq. (8), we plot r/R as a function of dimensionless time $C_1 t/\tau_c$ in log-log scale as depicted in Fig. 3(b). C_1 is a prefactor that covers the effect of discrepancies in the properties of fluids within the experimental settings. All the experimental data collapse into one single curve defined by Eq. (6). Figure 3(b) shows the capability of the developed correlation coupled with the prefactor C_1 to predict the spread of a liquid droplet surrounded by water or air.

Scaling of experimental data based on the transition length and time. In the drop coalescence experiments, Paulsen *et al.* [32–35] showed that experimental data can be scaled based on the transition time and radius, where all the data points collapse into a single curve. We found the transition time and radius from the experiments and scale the data in a similar

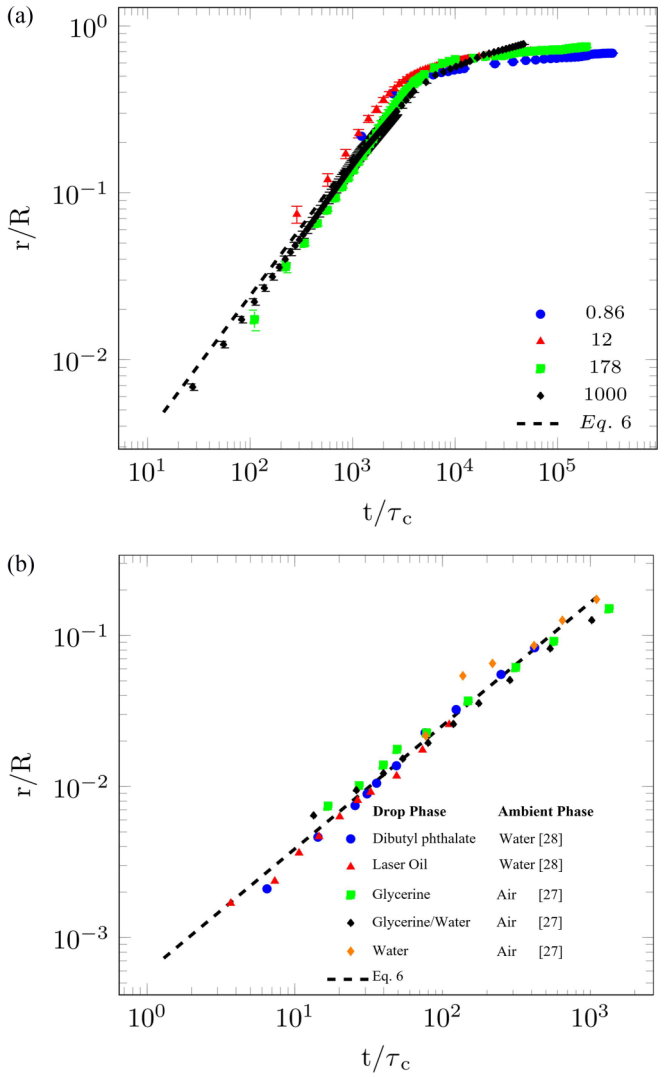

FIG. 3. (a) r/R as the function of t/τ_c and the resulting master curve. Blue, red, green, and black points are related to the fluid viscosity ratios of 0.86, 12, 178, and 1000, respectively. The black dashed line is the predicted values from Eq. (6). (b) r/R as a function of dimensionless time $C_1 t/\tau_c$. The experimental data and related fluid properties are collected from the literature for glycerin (1120 mPa s), glycerin-water (220 mPa s) and water droplet spreading in air [27], and dibutyl phthalate (16 mPa s) and laser oil (200 mPa s) droplet spreading in water [28]. The black dashed line is the predicted values from Eq. (6).

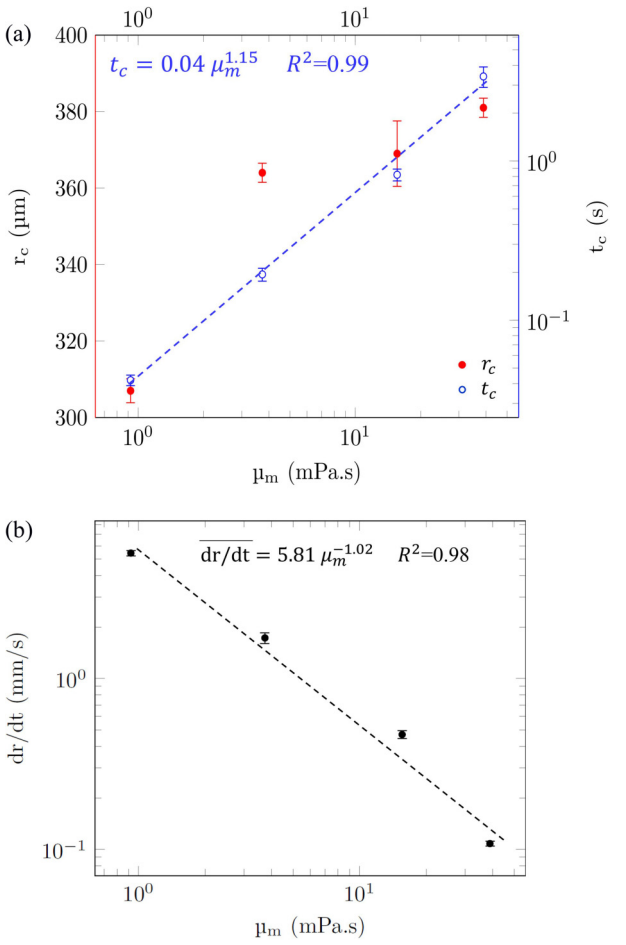

FIG. 4. (a) The transition radius and transition time as a function of the mean viscosity. The transition radii from the viscous regime to the inertial regime for 0.86, 12, 178, and 1000 are 307.1 ± 6.24, 364 ± 5, 369 ± 17.11, and $381 \pm 5\ \mu$m, respectively. The transition time depends on the viscosity of the ambient phase. For the viscosity ratios of 0.86, 12, 178, and 1000, the viscous regime lasts for 0.04, 0.19, 0.8, and 6 s, respectively. (b) The average contact line velocity as a function of the mean viscosity.

way. For each data set, we fit a straight line for the early time viscous regime [Fig. 2(b)]. The time (t_c) and radius (r_c) correspond to the deviation point from the fitted line. Figure 4(a) depicts the crossover (transition) radius (left axis) and transition time (right axis) from the viscous regime (end of the viscosity-dominated regime) as a function of the mean viscosity (μ_m). In the previous section [Fig. 2(d)], the crossover radius has a weak dependency on the viscosity ratios. A line fitted in Fig. 4(a) expresses the dependency of the transition time on the mean viscosity as defined in Eq. (9):

$$t_c = 0.04(\mu_m)^{1.15} \quad R^2 = 0.99. \tag{9}$$

Figures 2(d) and 4(a) and Eq. (1) suggest that the transition radii are weakly dependent on the outer fluid viscosity. In Eq. (8) for a constant trasition radius, the transition time increases linearly with the mean viscosity. A similar dependency from the experimental data is observed as presented in Fig. 4(a) and Eq. (9). In Fig. 4(b), we plot the average contact line velocity as a function of the mean viscosity. The velocities

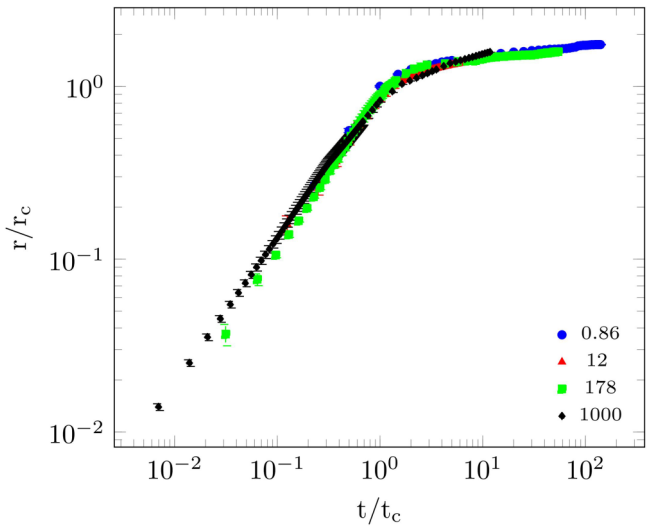

FIG. 5. The results of r/r_c as a function of t/t_c. All data collapse into a single master curve for spreading the water drop on a glass surface submerged in an oil phase.

are the average of (r,t) derivatives that are evaluated using the experimental data and central difference method. As expected, similar to Eq. (7), there is a linear dependency between the velocity and mean viscosity. The crossover radius and time [Fig. 4(a)] are used to rescale the growth of the wetted area. Figure 5 depicts the collapse of resultant radius growth curves into a master curve by scaling the data based on the transition time and radius.

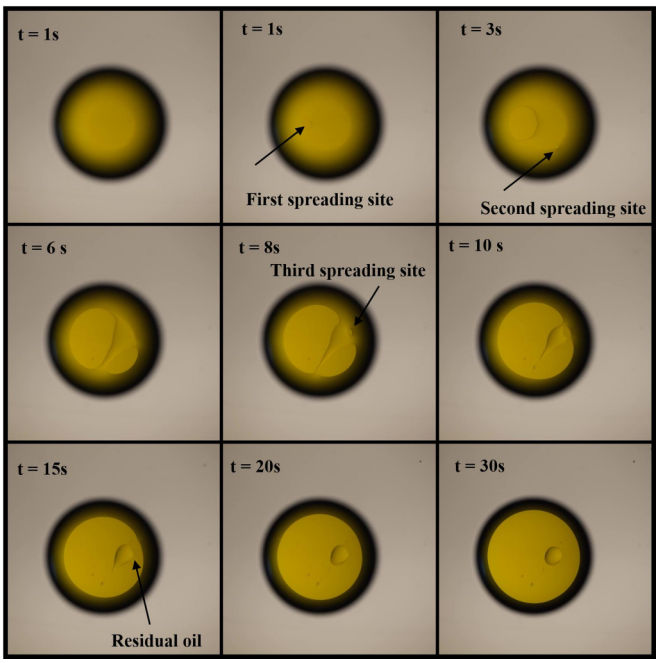

FIG. 6. Spreading of droplets at multiple points. The viscosity of the surrounding oil is 1000 mPa s. The first spreading initiates from a single rupture point. At $t = 3$ s, another rupture point touches the solid and spreads throughout the sites. The spreading continues through these points until a portion of the initial liquid (oil) is trapped between them ($t = 6$ s) and remains as a residual oil ($t = 15$ s).

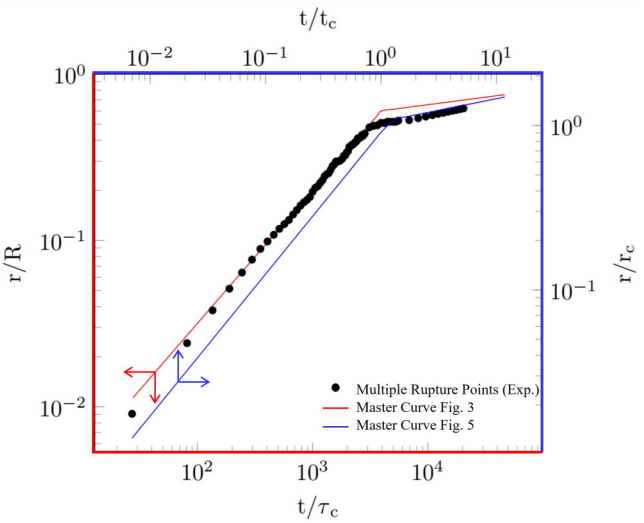

FIG. 7. Multipoint rupture spreading. The equivalent radius is plotted in black circles. The red line shows the predictive master curves from the dimensional analysis (left and bottom axis). The blue line is the master curve from scaling based on the transition time and length scales (right and top axis).

C. Spreading from multiple points

In previous analyses, the focus is on the wetting process beginning with a single rupture in the oil film. In this situation, there is no residual oil trapped under the water droplet within the wetted area. However, the initiation of spreading from multiple points may result in the entrapment of some quantities of oil underneath the water drop. In these experiments, the wetting starts from more than one single rupture point. Figure 6 shows the simultaneous motion of two contact lines. The key question is whether the master plot presented in Figs. 3 and 5 is also applicable for the nonideal dewetting systems in terms of irregular wetting patterns.

The wetted surface area is measured as a function of time and based on the equivalent radius being calculated. Figure 7 provides the equivalent radius as a function of time, shown in black circles. Master curves obtained from the dimensional analysis (Fig. 3) and that of transition length and time (Fig. 5) are also embedded in Fig. 7 in red and blue, respectively. It is revealed that the proposed master curve in Fig. 3 accurately predicts the growing wetted area (shown in red) while the one from transitional characteristics slightly underestimates the spreading dynamics from multiple points (shown in black) (Fig. 5).

IV. SUMMARY

Through experimental and scaling analysis, the effect of outer phase fluid viscosity on the spreading of water drops on a hydrophilic surface is investigated. De-ionized water is used as the drop phase wetting the untreated glass surfaces submerged in the bulk oil phase with various viscosities of 0.86, 12, 178, and 1000 mPa s. Oil film dewetting started from a single rupture point expanding circularly over time. It was found that at high viscosity ratio, the surrounding medium viscosity plays an important role in the spreading process. The growth rate of a wetted area follows two trends. Initially, the radius grows linearly in time ($r \sim t$), i.e., a viscosity-dominated regime. The growth rate of the wetted radius quickly reached ($r \sim t^{0.1}$), known as the Tanner regime. The transition time between the viscous regime and the Tanner regime was an increasing function of the outer fluid's viscosity, which could last for a few seconds for the oil with the viscosity of 1000 mPa s. It was demonstrated that the dynamic of drop spreading in liquid-liquid systems was similar to that of the liquid-air system. However, due to the higher viscosity of the surrounding phase, the spreading was slower and the duration of each regime was longer compared to the drop spreading in the air.

Using dimensional analysis, a correlation for the three-phase contact line velocity was found which could perfectly cover all viscosity ratios. It was revealed that for liquid-liquid systems, the spreading process is governed by both inner and outer fluid viscosities and scaled as $\mu_{out}^{0.53}\,\mu_{in}^{0.47}$. This is very close to the geometric mean of inner and outer viscosities $(\mu_{out}\mu_{in})^{0.5}$. It is clear that the transition radius from one regime to the other is weakly dependent on the viscosity ratios. The transition time from one regime to the other depends strongly on the viscosity ratios. Following the problem of drop coalescence, a scaling system was sought using the crossover points from the early time to late time dynamics as the characteristic length and time. As a result, a general master curve was obtained where all experimental data for all viscosity ratios perfectly fitted the unified curve. Finally, the dewetting dynamics of the oil film for a nonideal system, where the detachment starts from multiple points and some oil is trapped under the wetting phase, was further analyzed. It was shown that the wetting radius growth could be predicted by the developed master curves.

The developed master curves were capable of predicting the moving contact line in other experimental settings. However, the effect of inner fluid viscosity, fluid-fluid interfacial tension, and density differences between fluids should be evaluated before any generalizations. Moreover, numerical simulations of wetting dynamics can be utilized to extend the analysis to other systems.

ACKNOWLEDGMENT

The authors acknowledge financial support from the Canada Foundation for Innovation. This research was undertaken thanks in part to funding from the Natural Sciences and Engineering Research Council of Canada and the Canada First Research Excellence Fund.

[1] H. G. Döbereiner, B. Dubin-Thaler, G. Giannone, H. S. Xenias, and M. P. Sheetz, Dynamic Phase Transitions in Cell Spreading, Phys. Rev. Lett. **93**, 108105 (2004).

[2] R. Combes, M. Robin, G. Blavier, M. Aıdan, and F. Degreve, Visualization of imbibition in porous media by environmental scanning electron microscopy: Application to reservoir rocks, J. Pet. Sci. Eng. **20**, 133 (1998).

[3] R. Farajzadeh, A. Andrianov, R. Krastev, G. Hirasaki, and W. R. Rossen, Foam–oil interaction in porous media: Implications for foam assisted enhanced oil recovery, Adv. Colloid Interface Sci. **183–184**, 1 (2012).

[4] P. C. Myint and A. Firoozabadi, Thin liquid films in improved oil recovery from low-salinity brine, Curr. Opin. Colloid Interface Sci. **20**, 105 (2015).

[5] D. T. Wasan and A. D. Nikolov, Spreading of nanofluids on solids, Nature **423**, 156 (2003).

[6] I. Kobayashi, S. Mukataka, and M. Nakajima, Effects of type and physical properties of oil phase on oil-in-water emulsion droplet formation in straight-through microchannel emulsification, experimental and CFD studies, Langmuir **21**, 5722 (2005).

[7] I. Kobayashi, M. Nakajima, and S. Mukataka, Preparation characteristics of oil-in-water emulsions using differently charged surfactants in straight-through microchannel emulsification, Colloids Surf. A **229**, 33 (2003).

[8] R. Blossey, Self-cleaning surfaces—virtual realities, Nat. Mater. **2**, 301 (2003).

[9] R. Rioboo, M. Marengo, and C. Tropea, Time evolution of liquid drop impact onto solid, dry surfaces, Exp. Fluids **33**, 112 (2002).

[10] S. Jung, S. D. Hoath, and I. M. Hutchings, The role of viscoelasticity in drop impact and spreading for inkjet printing of polymer solution on a wettable surface, Microfluid. Nanofluid. **14**, 163 (2013).

[11] J. Kettle, T. Lamminmäki, and P. Gane, A review of modified surfaces for high speed inkjet coating, Surf. Coat. Technol. **204**, 2103 (2010).

[12] C. Huh and L. Scriven, Hydrodynamic model of steady movement of a solid/liquid/fluid contact line, J. Colloid Interface Sci. **35**, 85 (1971).

[13] J. C. Bird, S. Mandre, and H. A. Stone, Short-Time Dynamics of Partial Wetting, Phys. Rev. Lett. **100**, 234501 (2008).

[14] A. L. Biance, C. Clanet, and D. Quéré, First steps in the spreading of a liquid droplet, Phys. Rev. E **69**, 016301 (2004).

[15] T. Blake and J. Haynes, Kinetics of liquid-liquid displacement, J. Colloid Interface Sci. **30**, 421 (1969).

[16] R. Cox, The dynamics of the spreading of liquids on a solid surface. Part 1. Viscous flow, J. Fluid Mech. **168**, 169 (1986).

[17] L. Tanner, The spreading of silicone oil drops on horizontal surfaces, J. Phys. D: Appl. Phys. **12**, 1473 (1979).

[18] T. Blake, A. Clarke, J. De Coninck, and M. J. De Ruijter, Contact angle relaxation during droplet spreading: comparison between molecular kinetic theory and molecular dynamics, Langmuir **13**, 2164 (1997).

[19] T. Blake and J. De Coninck, The influence of solid–liquid interactions on dynamic wetting, Adv. Colloid Interface Sci. **96**, 21 (2002).

[20] M. J. De Ruijter, M. Charlot, M. Voué, and J. De Coninck, Experimental evidence of several time scales in drop spreading, Langmuir **16**, 2363 (2000).

[21] D. Duvivier, D. Seveno, R. Rioboo, T. Blake, and J. De Coninck, Experimental evidence of the role of viscosity in the molecular kinetic theory of dynamic wetting, Langmuir **27**, 13015 (2011).

[22] M. Fermigier and P. Jenffer, An experimental investigation of the dynamic contact angle in liquid-liquid systems, J. Colloid Interface Sci. **146**, 226 (1991).

[23] S. Goossens, D. Seveno, R. Rioboo, A. Vaillant, J. Conti, and J. De Coninck, Can we predict the spreading of a two-liquid system from the spreading of the corresponding liquid–air systems?, Langmuir **27**, 9866 (2011).

[24] D. Seveno, T. Blake, S. Goossens, and J. De Coninck, Predicting the wetting dynamics of a two-liquid system, Langmuir **27**, 14958 (2011).

[25] R. T. Foister, Three-phase boundary expansion in thin liquid films, J. Colloid Interface Sci. **116**, 109 (1987).

[26] R. T. Foister, The kinetics of displacement wetting in liquid/liquid/solid systems, J. Colloid Interface Sci. **136**, 266 (1990).

[27] A. Eddi, K. G. Winkels, and J. H. Snoeijer, Short time dynamics of viscous drop spreading, Phys. Fluids **25**, 013102 (2013).

[28] S. Mitra and S. K. Mitra, Understanding the early regime of drop spreading, Langmuir **32**, 8843 (2016).

[29] R. W. Hopper, Plane Stokes flow driven by capillarity on a free surface, J. Fluid Mech. **213**, 349 (1990).

[30] J. Eggers, J. R. Lister, and H. A. Stone, Coalescence of liquid drops, J. Fluid Mech. **401**, 293 (1999).

[31] D. G. Aarts, H. N. Lekkerkerker, H. Guo, G. H. Wegdam, and D. Bonn, Hydrodynamics of Droplet Coalescence, Phys. Rev. Lett. **95**, 164503 (2005).

[32] J. D. Paulsen, J. C. Burton, and S. R. Nagel, Viscous to Inertial Crossover in Liquid Drop Coalescence, Phys. Rev. Lett. **106**, 114501 (2011).

[33] L. Duchemin, J. Eggers, and C. Josserand, Inviscid coalescence of drops, J. Fluid Mech. **487**, 167 (2003).

[34] W. Yao, H. Maris, P. Pennington, and G. Seidel, Coalescence of viscous liquid drops, Phys. Rev. E **71**, 016309 (2005).

[35] J. D. Paulsen, R. Carmigniani, A. Kannan, J. C. Burton, and S. R. Nagel, Coalescence of bubbles and drops in an outer fluid, Nat. Commun. **5**, 3182 (2014).

[36] K. G. Winkels, J. H. Weijs, A. Eddi, and J. H. Snoeijer, Initial spreading of low-viscosity drops on partially wetting surfaces, Phys. Rev. E **85**, 055301 (2012).

[37] J. Masliyah, Z. J. Zhou, Z. Xu, J. Czarnecki, and H. Hamza, Understanding water-based bitumen extraction from Athabasca oil sands, Can. J. Chem. Eng. **82**, 628 (2004).

[38] J. M. Nordbotten, M. A. Celia, S. Bachu, and H. K. Dahle, Semianalytical solution for CO_2 leakage through an abandoned well, Environ. Sci. Technol. **39**, 602 (2005).

[39] See Supplemental Material at http://link.aps.org/supplemental/10.1103/PhysRevE.97.063104 for sequential water drop spreading images as a function of the outer phase viscosity and the relation between dimensionless groups dictating the spreading dynamics.

[40] A. Carlson, G. Bellani, and G. Amberg, Universality in dynamic wetting dominated by contact-line friction, Phys. Rev. E **85**, 045302 (2012).